Determination of diffusion coefficients of mercury atoms in various gases from longitudinal spin relaxation in magnetic gradients

B. Clément [1], M. Guigue [2], A. Leredde,[1] G. Pignol [1,*], D. Rebreyend,[1] S. Roccia,[1] and S. Touati [1]

[1]*Université Grenoble Alpes, CNRS, Grenoble INP, LPSC-IN2P3, 38000 Grenoble, France*
[2]*Sorbonne Université, Université Paris Cité,*
CNRS/IN2P3, Laboratoire de Physique Nucléaire et de Hautes Énergies (LPNHE), 75005 Paris, France

We present a method to measure the binary diffusion coefficient of mercury atoms in a gas at room temperature and low pressure. It is based on the measurement of the longitudinal spin relaxation of optically pumped mercury-199 atoms in a magnetic field gradient. We provide a consistent set of diffusion coefficients for helium-3, helium-4, argon, krypton, xenon, nitrogen, carbon dioxide, oxygen, and air.

I. INTRODUCTION

Nuclear magnetic resonance (NMR) provides a versatile and powerful probe of diffusion phenomena. In their seminal work in 1954, Carr and Purcell [1] determined the self-diffusion coefficient of ordinary water by measuring the decay of transverse spin polarization in a magnetic field gradient. Variants of this technique, such as pulsed gradient spin echo, are now routinely used to measure diffusion coefficients in liquids, which are of the order of 10^{-5} cm^2/s. In gases, although diffusion NMR experiments are less ubiquitous, diverse techniques have been employed with hyperpolarized noble gases to measure the diffusion coefficient of helium-3 [2–5] or xenon-129 [6,7] in different gases. Compared to the case of liquids, the diffusion is much faster in gases, of the order of 0.1 cm^2/s at standard temperature and pressure.

In this article we report on a study of the diffusion of mercury atoms in various gases at room temperature (20 °C). In the present experiment, the mercury is polarized in a very low field with optical pumping in a cell filled with mercury-199 at a partial pressure of about 10^{-5} mbar. In addition the cell contains a buffer gas at a pressure in the range $0.5 - 5$ mbar. In such a situation, the mercury atoms diffuse in the cell in a very short time, about 10 ms. Contrary to the case of liquids, for which the diffusion time across a sample of size 1 cm is about 10^5 s, the mercury atoms explore the entire cell many times during the measurement duration of a few seconds. We have developed a method to determine the diffusion coefficient in this "motion narrowing" regime, based on the measurement of the longitudinal relaxation rate (rather than the decay of the transverse polarization in most NMR diffusion experiments) in an applied magnetic field gradient.

The motivation for this work comes from the prospects for a precision measurement of the gyromagnetic ratio of mercury-199 using helium-3 as a comagnetometer in the same cell. The helium-3 will be polarized by metastable-exchange optical pumping and its precession will be read out with induction coils. This technique is adequate for helium-3 operating in the millibar pressure range. Then, the presence of the helium-3 buffer gas will increase the time it takes for mercury atoms to average the field over the cell. In such a situation the residual magnetic field gradients could significantly shorten the decay time of the precession signal, and therefore affect the precision of the measurement of the Larmor precession frequency. In order to quantify the requirement on the acceptable field uniformity in the experiment, a dedicated measurement of the diffusion coefficient of mercury in helium-3 is desired.

The rest of the article is organized as follows. In Sec. II we review the treatment of longitudinal relaxation of the spins (i.e., the decay of the longitudinal component of the polarization) due to field gradients. The experimental apparatus and the analysis procedure are described in Secs. III and IV. In Sec. V we present our results for the binary diffusion coefficient of mercury in various gases (helium-3, helium-4, argon, krypton, xenon, nitrogen, carbon dioxide, oxygen, and air) and compare them with previous measurements using non-NMR methods (see Ref. [8] for a comprehensive review) and the predictions based on Chapman-Enskog theory.

II. LONGITUDINAL RELAXATION DUE TO FIELD GRADIENT

Consider an ensemble of polarized spin 1/2 atoms confined in a cell exposed to a nonuniform magnetic field. Due to their random motion through the cell, each atom effectively sees a fluctuating magnetic field, resulting in depolarization of the ensemble [9–17]. In the motional narrowing case, i.e., when the depolarization is slow compared with the correlation time τ_D of the fluctuating field, the longitudinal and transverse polarization decay exponentially with relaxation rates Γ_1 and Γ_2 given by Redfield's theory [13]. In sufficiently high holding magnetic field B, that we take along the x axis, the longitudinal relaxation rate due to the nonuniformity of the magnetic field is given by

$$\Gamma_1 = D \frac{G^2}{B^2}, \tag{1}$$
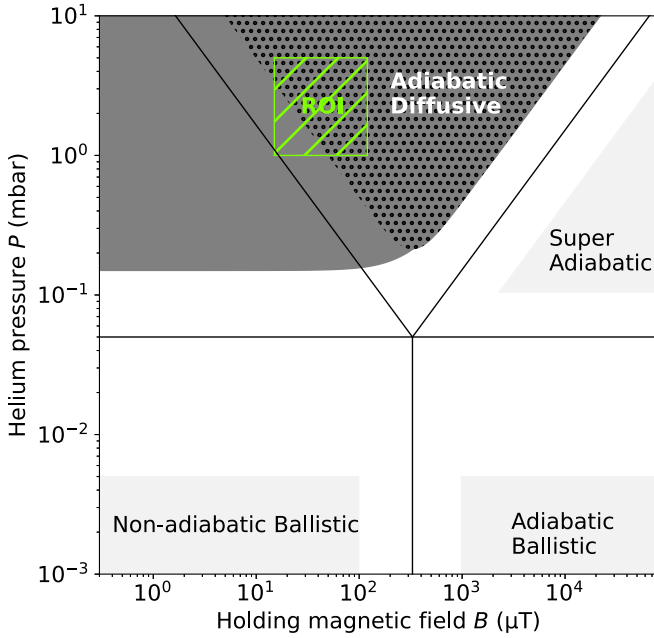
*guillaume.pignol@lpsc.in2p3.fr

FIG. 1. Different regimes for the longitudinal relaxation of mercury atoms in a helium buffer gas. The horizontal line corresponds to the separation between diffusive and ballistic regimes. The upper gray zone corresponds to the validity domain of Eq. (2), including the dotted region corresponding to the validity domain of Eq. (1). The chartreuse dashed region, marked ROI, corresponds to the parameter space explored experimentally in this study.

where D is the diffusion coefficient and G is the gradient of the transverse field components, more precisely $G^2 = \langle (\vec{\nabla} B_y)^2 + (\vec{\nabla} B_z)^2 \rangle$ [18].

Let us now discuss in detail the validity condition of Eq. (1). For that, we consider for definiteness a cell of cylindrical shape, of radius $R = 2$ cm and length $L = 10$ cm, filled with a mixture of mercury and helium-4 atoms at room temperature. The helium pressure P and the value of the holding magnetic field B define different regimes for the longitudinal relaxation, shown in Fig. 1.

First let us consider the pressure. Without helium, mercury atoms would have a ballistic motion in the cell, with a time between two wall collisions set by $2R/v \approx 0.4$ ms, $v = 11$ cm/ms being the thermal velocity of mercury atoms at room temperature. Note that atomic collisions between two mercury atoms are much less frequent than wall collisions, because the pressure of mercury atoms in the cell needs to be very low (about 10^{-5} mbar in our experiment and in any case below the vapor pressure of 2×10^{-3} mbar at room temperature). Now, for sufficiently large pressure P of helium in the cell, the mercury atoms undergo diffusive motion characterized by the diffusion coefficient D inversely proportional to P, and the diffusion time across the cell is set by $\tau_D = R^2/D$. This time is much longer than the time it would have taken to cross the cell in pure ballistic motion, so that the diffusive regime holds for $\tau_D \gg 2R/v$, i.e., $D \ll vR/2$. For helium in our specific cell this corresponds to $P \gg 0.05$ mbar, i.e., the upper part of the parameter space in Fig. 1.

In the diffusive regime, the spectral density of the fluctuating magnetic field seen by the atoms randomly moving in

a static gradient can be derived from the diffusion equation. Then, following McGregor [15], the Redfield theory of relaxation can be applied to yield expressions for the relaxation rate, which depends on the geometry of the cell and the shape of the magnetic field. We derive in detail in the Appendix an expression adequate for the case of our study:

$$\Gamma_1 = D \frac{G^2}{B^2} \sum_{k=1}^{\infty} \frac{(\gamma B \tau_D)^2}{(\gamma B \tau_D)^2 + x_{1k}^4} \frac{2}{x_{1k}^2 - 1}, \qquad (2)$$

where γ is the gyromagnetic ratio ($\gamma = 2\pi \times 7.6$ Hz/μT for mercury-199) and x_{1k} is the kth zero of the derivative of the Bessel function J_1. In fact, Eq. (2) becomes invalid at high Larmor frequency γB because the correlation function is not described by the diffusion equation for times shorter than the time between two atomic collisions $\tau_c = 4D/v^2$. The validity domain of Eq. (2) is represented by the upper gray zone in Fig. 1.

At moderate field B, specifically $\gamma B \tau_D \gg 1$ and $\gamma B \tau_c \ll 1$ (corresponding to the dark dotted zone in Fig. 1 labeled *adiabatic diffusive*), the general expression (2) simplifies to the formula (1). Physically, this regime is such that there are many atomic collisions in one Larmor time $(\gamma B)^{-1}$, but many Larmor times during the time τ_D it takes to traverse the cell diffusively. In the adiabatic diffusive regime, the relaxation rate becomes independent of the geometry of the cell [18]. This is an advantage for determination of the diffusion coefficient, because it reduces systematic errors due to the imperfections of the geometry of the cell.

The rectangular region marked with dashes in Fig. 1 is our region of interest, corresponding to the parameters used in the experiment. Conceptually, the experiment consists of filling a cell with a mixture of mercury and a gas with a controlled pressure, applying a known field B and a known gradient G, measuring the relaxation rate Γ_1, and deducing an effective diffusion coefficient D_{eff} defined by

$$\Gamma_1(G) \equiv D_{\text{eff}} \frac{G^2}{B^2} + \Gamma_1(0). \qquad (3)$$

It is actually necessary to measure Γ_1 as a function of the applied gradient in order to separate the magnetic relaxation from the other sources of relaxation $\Gamma_1(0)$. In the region of interest, the effective diffusion coefficient departs from the true coefficient D by up to 30%, which is larger than the accuracy of the measurement (about 1%, as we will see). In fact, based on Eq. (2), we have

$$D_{\text{eff}} = \sum_{k=1}^{\infty} \frac{D}{1 + \left(\frac{D}{\gamma B R^2}\right)^2 x_{1k}^4} \frac{2}{x_{1k}^2 - 1}. \qquad (4)$$

In practice, as will be explained later, for a given cell D_{eff} was measured for different values of the holding field B, then Eq. (4) was used to extract the true diffusion coefficient D.

III. EXPERIMENTAL SETUP

The experimental setup is composed of three parts: a 253.7 nm laser; a system generating magnetic fields and gradients, which are both schematized in Fig. 2; and a cell filling station, shown in Fig. 3.
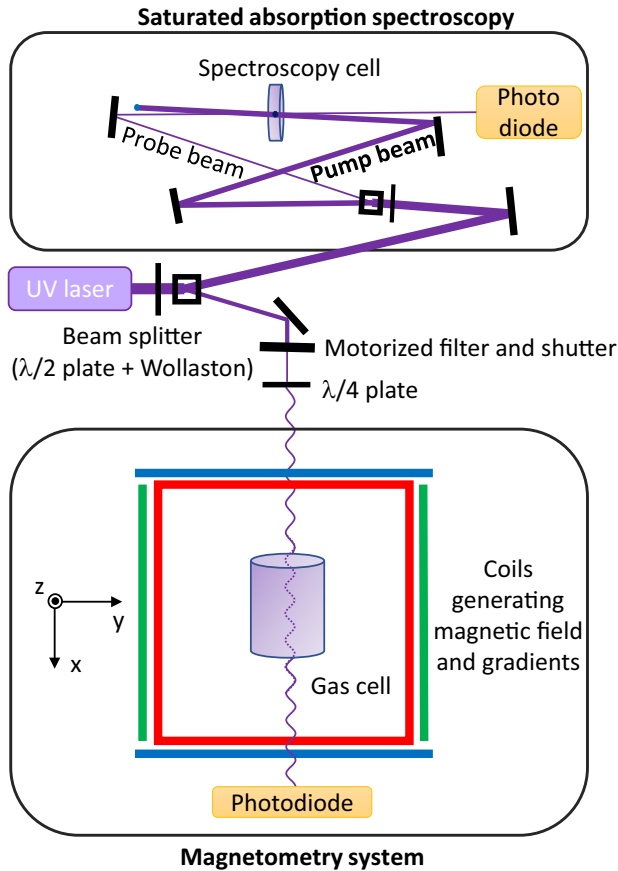
FIG. 2. A schematic representation of the laser and magnetometry setups. The initial beam is split in two linearly polarized beams. The top one serves for locking the laser frequency on the mercury-199 $F = 1/2$ transition obtained through saturated absorption spectroscopy. The bottom one is circularly polarized with a quarter-wave plate and is used for optical pumping and precession measurements.

The ground level $^1S_0$ of mercury-199 has a total spin $F = 1/2$ arising only from the nuclear spin. The excited $^3P_1$ level at 253.7 nm is split in two hyperfine sublevels, $F = 1/2$ and $F = 3/2$, separated by 22 GHz. Mercury atoms can be polarized by optical pumping on the $F = 1/2$ to $F = 1/2$ transition. A 253.7 nm TOPTICA TA-FHG pro laser is used to realize the optical pumping. It consists of an infrared laser diode coupled to two frequency doubling nonlinear crystals. A grating allows for a fine variation of the laser frequency around the resonance. Saturated absorption spectroscopy provides a reference to lock the laser on the precise frequency of the $F = 1/2$ to $F = 1/2$ transition of mercury-199. The laser output power is at maximum 20 mW. The beam is split in two, most of the power is used for the laser locking scheme, and only 30–60 μW are used for the experiment itself. Using half-wave and quarter-wave plates, the laser beam is polarized circularly for the experiment. A motorized filter and a shutter allow for fast (a few tens of milliseconds) variation of the beam intensity. The polarized beam is directed through a spectroscopy cell filled with mercury and a few millibar of buffer gas.

Our experimental cell is placed at the center of three pairs of orthogonal square coils. Each pair of coils is capable of
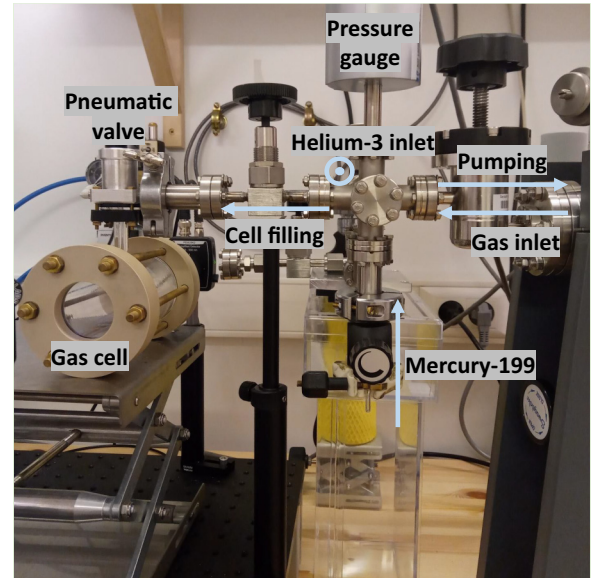

FIG. 3. Photograph of the cell filling station, with the magnetometry cell connected. The arrows indicates the various gas flows allowed within the system.

generating a magnetic field up to 200 μT. The coils are used to cancel the ambient magnetic field, set the fields for optical pumping and free precession, and generate magnetic gradients. We generate the magnetic gradient by controlling separately the current in the two coils forming the x pair. In the volume of the cell the magnetic field takes the form

$$\vec{B}(x, y, z) = \begin{pmatrix} B_x(0) \\ B_y(0) \\ B_z(0) \end{pmatrix} + G_x \begin{pmatrix} x \\ -y/2 \\ -z/2 \end{pmatrix}. \quad (5)$$

When the field is set along the x axis, the depolarizing gradient in Eq. (2) is $G = \sqrt{(\vec{\nabla}B_y)^2 + (\vec{\nabla}B_z)^2} = \frac{G_x}{\sqrt{2}}$. We performed a magnetic mapping in the central region (without the cell) to calibrate the magnetic generation system before the experiment, and repeated the mapping after the experiment. The uncertainty on the set field is $\Delta B_x = 0.5\,\mu$T and the relative uncertainty on the set gradient is $\Delta G_x/G_x = 1\%$. As the coil power supplies are unipolar, the maximum gradient that can be applied is imposed by the earth's magnetic field, and goes from $G_x = \pm 300$ nT/cm at $B_x = 15\,\mu$T to $G_x = \pm 1400$ nT/cm at $B_x = 120\,\mu$T. After crossing the cell, the light is detected using a photodiode whose signal is digitized through a 16-bit analog-to-digital converter (ADC). NI LABVIEW is used to integrate and coordinate the control of the various subsystems: field and gradient generation, UV light intensity, and data recording.

The cell used in the experiment is a 10-cm-long glass cylinder with an internal diameter of 4 cm. It is closed on both ends with quartz windows. A small glass tube ended with a pressure-controlled valve allows to connect the cell to a filling station through a KF16 flange. The filling station consists of a small volume to which several items isolated by valves are connected: a turbo pump to empty the whole system, a pressure gauge, a small volume containing a droplet of enriched mercury-199, and two gas inlets. The valve for

these last devices allows for a fine control of the opening, allowing to adjust precisely the pressure of gas within the system. One inlet is connected to a small helium-3 bottle that is never removed, whereas the gas bottle on a second inlet can be changed. The pressure gauge is a capacitance manometer that gives absolute measurements with a microbar accuracy in the microbar to tens of millibar range, independently of the nature of the gas. To prepare a cell, the full system is first evacuated, then filled with the desired gas, close to the targeted pressure. The valve to the mercury droplet is then opened and we wait for mercury at saturated vapor pressure (at ambient temperature) to diffuse into the cell. The quantity of mercury is controlled through the absorption of UV light. When the absorption is within $45\% \pm 5\%$, the cell is isolated and disconnected from the filling station. Either the pneumatic valve or the toric seals at the cell windows have small leaks. These leaks are monitored by measuring the pressure within the cell at the end of each measurement.

IV. ANALYSIS PROCEDURE

A. Data taking strategy

The basic element of the data taking is a sequence for a set of parameters (τ, B_x, G_x) consisting of:

(1) Optical pumping at 60 μW, with a holding magnetic field along the x axis (of magnitude B_x) for 8 s;

(2) Closure of the beam shutter and setting of a magnetic gradient G_x along the x axis over 0.2 s;

(3) Relaxation during a time τ in the dark; it is during this time that the depolarization we want to measure occurs;

(4) Opening of the beam shutter with the gradient at zero and setting of a field along the z axis (of magnitude $B_z = 40 \mu$T). We take care that during the transition, the magnetic field never goes to zero to avoid depolarization. The change of direction over 0.4 s of the magnetic field is fast enough so the polarization stays along the x axis and can precess in the xy plane;

(5) Recording of the precession signal in the 40 μT field for 3 s, with a light power reduced to 30 μW;

(6) Setting of the field to zero to depolarize the mercury atoms.

The time structure of a sequence is illustrated in Fig. 4. The analysis of each sequence will give a value of the polarization after a dark time τ. Five consecutive sequences make a τ scan for a set (B_x, G_x) with varying dark time. From a τ scan one extracts a value of Γ_1. Using short τ scans of 2–2.5 min makes the analysis insensitive to drifts of the laser intensity as well as variations of the cell absorption which have a larger timescale. A set of seven consecutive τ scans for a fixed B_x, varying G_x, is a gradient scan from which we extract a value of D_{eff}. A gradient scan lasts for approximately 15 min, making the analysis insensitive to slow drifts of the ambient field. A full run is a collection of gradient scans performed several times for each value of B_x.

B. Precession signals and extraction of the polarization from a sequence

In order to extract the longitudinal relaxation rate Γ_1 from a τ scan, the polarization p of the atoms at the beginning of the
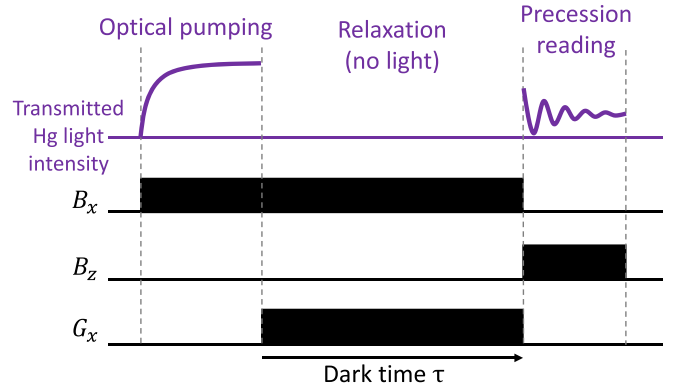

FIG. 4. General time structure of the polarization measurement sequence for the transmitted laser intensity, the magnetic field and the gradient. The transitions between the main steps are not indicated.

precession must be measured from sequences with different values of dark times τ, as shown in Fig. 4. The precession signal, that is, the power of the transmitted light, is not a simple damped-oscillator signal, but is given by

$$S(t) = S_0 \exp\{ -n_{\text{Hg}}\sigma_{\text{Hg}}[1 + p_\parallel(t)]L\}, \qquad (6)$$

where S_0 is the light power entering the cell, n_{Hg} the Hg atoms density in the cell, σ_{Hg} the light absorption cross section, and L the optical path length, and $p_\parallel(t)$ is the instantaneous projection along the beam of the precessing atomic polarization:

$$p_\parallel(t) = p \cos(\gamma B_z t) e^{-\Gamma_2 t}. \qquad (7)$$

Here Γ_2 accounts for the decay of the transverse polarization during the precession. Then, the polarization p is obtained from the ratio of the maximum S_{max} to minimum S_{min} of the signal S by

$$p = \frac{\ln \frac{S_{\text{max}}}{S_{\text{min}}}}{-\ln(1 - A)}. \qquad (8)$$

In the expression (8), $A = 1 - \exp(-n_{\text{Hg}}\sigma_{\text{Hg}}L)$ is the total absorption of the cell with unpolarized atoms, which is measured at the beginning (and also at the end) of the run when filling the cell.

For each run, we provide a file in the Supplemental Material [19] with the results of the analysis of each sequence, including in particular S_{min} and S_{max}.

C. Extraction of the longitudinal relaxation rate from a τ scan

The polarization p is measured for several dark times τ in order to produce a τ scan. Figure 5 shows an example of τ scan for a given configuration of magnetic field for a cell of helium-4 at 1 mbar. An exponential model is then fitted to extract the relaxation rate Γ_1 for each τ scan.

D. Extraction of D_{eff} from a gradient scan

The extraction of the longitudinal relaxation rate is repeated for several values of transverse magnetic gradients G while keeping the same value of the holding magnetic field B_x. Figure 6 shows the relaxation rate Γ_1 obtained for seven
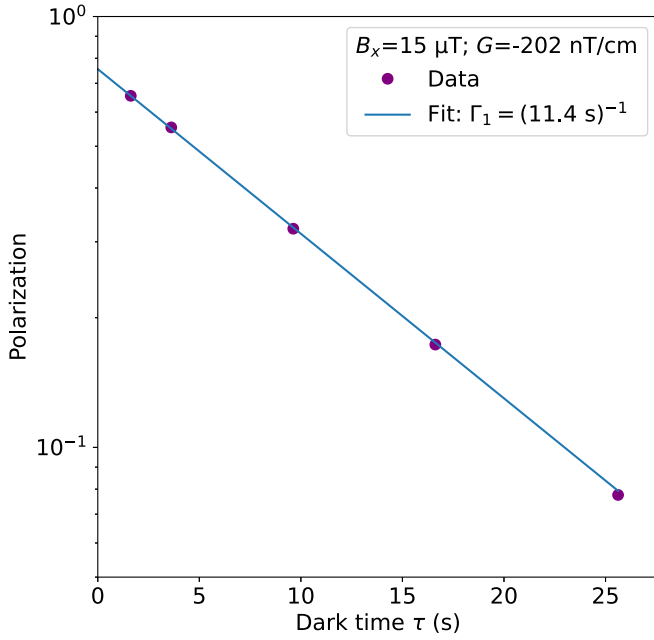
FIG. 5. Example of polarization evolution with the dark time for a holding magnetic field of 15 μT and a gradient of -202 nT/cm. The cell is filled with 1 mbar of helium-4. The time constant Γ_1 of the exponential model is obtained by fitting the data.

values of magnetic field gradient between -290 nT/cm and 290 nT/cm.

This collection of measurements represents a parabola whose curvature corresponds to the diffusion coefficient D_{eff} described in Eq. (3). In fact, we fit with a general parabola using

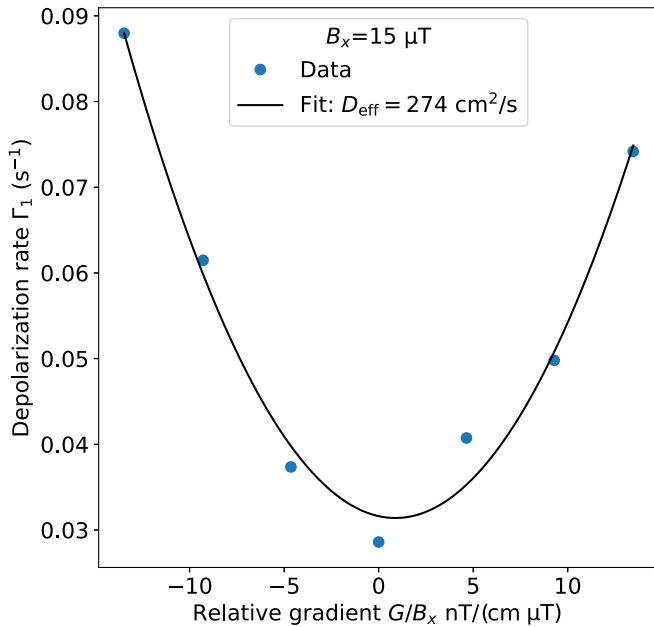$$\Gamma_1(G) = \Gamma_1(0) + C \times \frac{G}{B_x} + D_{\mathrm{eff}} \times \frac{G^2}{B_x^2}, \qquad (9)$$

FIG. 6. Longitudinal relaxation rate Γ_1 extracted from a gradient scan for a cell of 1 mbar of helium-4 as a function of the relative transverse gradient G/B_x. Data are fitted using Eq. (9) to extract D_{eff}.

TABLE I. Gradient-independent relaxation time $1/\Gamma_1(G=0)$ and diffusion coefficient D extracted from each run. The correction applied to each value (right column) is detailed in Sec. IV E.

Gas	Initial pressure (mbar)	$1/\Gamma_1(G=0)$ (s)	D (cm^2/s)	Corrected D (cm^2/s)
^{3}He	1.0	39.7(3)	578(10)	617(12)
^{3}He	2.0	40.3(3)	267(5)	289(6)
^{3}He	5.0	43.5(4)	119(6)	121(6)
^{4}He	1.0	34.6(4)	495(9)	519(10)
^{4}He	2.0	36.4(1)	262(5)	265(5)
^{4}He	5.0	36.6(1)	105(4)	107(4)
Ar	1.0	39.2(5)	110(7)	111(7)
Ar	1.0	38.5(4)	111(7)	112(7)
Kr	0.5	36.1(1)	149(8)	150(8)
Kr	1.0	36.4(3)	75(5)	75(5)
Xe	0.5	39.4(6)	106(5)	107(5)
Xe	1.0	41.2(3)	41(5)	41(4)
N_2	0.5	34.2(4)	257(7)	265(7)
N_2	1.0	37.7(4)	115(6)	116(6)
N_2	2.0	35.8(4)	71(4)	73(4)
N_2	2.0	43.9(6)	57(5)	57(5)
CO_2	0.5	44.2(4)	174(5)	178(5)
CO_2	1.0	42.6(4)	90(6)	91(6)
O_2	0.2	7.22(8)	577(35)	598(37)
O_2	0.3	4.63(4)	339(76)	340(77)
Air	0.5	9.50(4)	235(10)	243(11)
Air	1.0	5.40(5)	88(28)	89(29)
Air	1.0	5.73(5)	177(18)	180(19)

where $\Gamma_1(0)$, and C and D_{eff} are the adjusted parameters. The coefficient $\Gamma_1(0)$ corresponds to all the field-independent depolarization processes, such as the collision of the Hg with the cell walls or with other atoms in the gas. It also includes the small magnetic relaxation rate contribution induced by magnetic gradients produced by and proportional to the holding magnetic field. The linear term C is the cross-term that accounts for a possible offset of the magnetic gradient; after the analysis this term is found to be compatible with zero. The average values of $1/\Gamma_1(0)$ for each run are listed in Table I. The values are all similar and of the order of 40 s except for O_2 and air, due to the paramagnetic nature of the oxygen molecule.

E. Extraction of D from a run

As shown in Fig. 7, for a given run, we get several values of D_{eff} for each value of the holding magnetic field B_x (black circles), that we average to get the red dots. The previous fits are performed using a linear regression, with all the points having the same weights, and no errors are computed. For a given holding field, the error on the average D_{eff} in Fig. 7 is computed from the standard deviation of D_{eff} divided by the square root of the numbers of measurement. This error captures the statistical precision as well as the imperfections of the fitting procedure.

The number of repetitions for each holding field value B_x was optimized in order to have an almost identical statistical error for each point. The statistical fluctuation on the parameter D_{eff} increases with B_x since the possible range of G/B_x
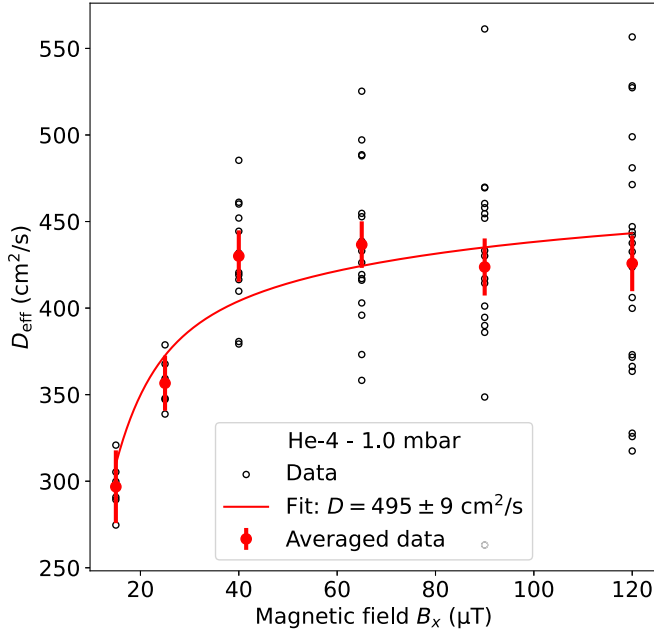
FIG. 7. Parameter D_{eff} obtained from several gradient scans as a function of the holding magnetic field B_x for a 1 mbar helium-4 cell (black circles). The red dots represent the average value and error for each B_x. Model (4) (red line) is fitted to the data in order to extract the diffusion coefficient D.

gets smaller with larger B_x. In addition, the magnetic field and gradient are not perfectly known, which leads to systematic errors on the extracted D_{eff}. The error bars represented on the averaged values of D_{eff} (red dots) include both statistical and systematic errors in quadratic sum.

Finally, we can extract the value and error of the parameter D from Eq. (4) by fitting this model to the data of each run using a χ^2 minimization method. Table I presents the extracted diffusion coefficient D for each run. Figures analogous to Fig. 7 are provided in the Supplemental Material [19] for all the runs.

The cell is known to leak with the pressure increasing linearly over time at an approximate rate of 0.8 μbar/h. The average quantity of air in the cell over the measurement is determined by recording the pressure within the cell before and after the measurement. We consider a stagnant mixture of mercury in some gas at partial pressure P_{gas} with an additional quantity of air (treated as a single species) at partial pressure P_{air}. The concentration of mercury is negligible with respect to the other gases. Then the effective diffusion coefficient of mercury in the mixture is [20]

$$\frac{P_{\text{mix}}}{D^{\text{mix}}(P_{\text{mix}})} \approx \frac{P_{\text{air}}}{D^{\text{air}}(P_{\text{mix}})} + \frac{P_{\text{gas}}}{D^{\text{gas}}(P_{\text{mix}})}, \qquad (10)$$

where $P_{\text{mix}} = P_{\text{air}} + P_{\text{gas}}$ is the total pressure of the mixture. As $D(P)P$ is a constant, inverting this formula relates the diffusion coefficient of mercury in the gas $D^{\text{gas}}(P_{\text{gas}})$ to the measured $D^{\text{mix}}(P_{\text{mix}})$:

$$\frac{1}{D^{\text{gas}}(P_{\text{gas}})} = \frac{1}{D^{\text{mix}}(P_{\text{mix}})} - \frac{P_{\text{air}}}{D^{\text{air}}(P_0)P_0}, \qquad (11)$$

TABLE II. Comparison between the diffusion coefficient D extracted from our measurements, theory (Chapman-Enskog), and other results from the literature. The values displayed with an asterisk [21] are a combination of other measurements. The values expressed in cm^2/s are extrapolated at 1 mbar pressure and 293 K.

Gas	This work	Theory	Literature
^{3}He	598(8)	786	
^{4}He	523(7)	693	566 [22]
Ar	111(5)	113	113 [22], 147 [23]
Kr	75(3)	70	69(4) [24]
Xe	64(4)	50	49(3) [24]
N_2	129(3)	129	145 [22], 121(9) [24], 138* [21]
CO_2	89(2)	80	113 [22]
O_2	118(7)	123	
Air	125(5)	128	136* [21]
Air$^{\text{a}}$	126(3)	–	–

$^{\text{a}}$This value is obtained by combining our measurements of nitrogen, oxygen, argon, and carbon dioxide.

where the diffusion coefficient $D^{\text{air}}(P_0)$ at some reference pressure P_0 is measured independently. The diffusion coefficients corrected using Eq. (11) are reported in the last column of Table I. We use the combination of the measurements of diffusion coefficient in air listed in Table II to implement this correction. The error on this measurement is propagated on all the final results. As there are three independent measurements for air, all three are slightly modified by this correction but the overall combination is not.

V. RESULTS AND DISCUSSION

For each gas, several runs have been performed for different gas pressures, as summarized in Table I. The dependency as an inverse of the pressure is verified, and we combine all available data for each gas to compute the diffusion coefficient for a pressure of 1 mbar. These are reported in Table II.

A theoretical model for binary diffusion coefficients can be obtained from the kinetic theory of gases. The formula derived independently by Chapman and Enskog [20,25,26] relies on a Lennard-Jones interaction with parameters $\sigma = \sigma_1 + \sigma_2$ and $\varepsilon = \sqrt{\varepsilon_1 \varepsilon_2}$, where σ_1, σ_2, and ε_1, ε_2 are, respectively, the diameter and the depth of the individual Lennard-Jones potential for each species. The Chapman-Enskog formula is then

$$D = \frac{3kT}{8P\pi\sigma^2\Omega^*(\varepsilon/T)} \left(\frac{\pi kT(m_1 + m_2)}{2m_1 m_2} \right)^{\frac{1}{2}}, \qquad (12)$$

where m_1 and m_2 are the masses of the two species, T the temperature, and Ω^* the collision integral, quantifying the correction from the hard sphere model, which depends on the depth of the Lennard-Jones potential and the temperature. To compute the values given in Table II, we use the Lennard-Jones parameters derived from viscosity data listed in Ref. [25] and the Ω^* tabulated in Ref. [20].

Our measurements are in rather good agreement with the theoretical calculations, except for helium. This is to be expected, as Lennard-Jones potential does not model correctly the behavior of mercury helium mixture [27].

Nevertheless, the ratio of diffusion coefficient between helium-3 and helium-4 should only depend on the masses:

$$r^2 = \left(\frac{D^{^3\text{He}}}{D^{^4\text{He}}}\right)^2 \approx \frac{m_{^4\text{He}}}{m_{^3\text{He}}} \approx 1.33. \tag{13}$$

Indeed, our measurement leads to $r^2 = 1.31 \pm 0.05$, which is in agreement with the expected value.

We also report in Table II the results of other measurements (using non-NMR methods) available in the literature. The values are extrapolated to the temperature of 293 K using the Chapman-Enskog temperature dependence $\frac{1}{\Omega^*}T^{\frac{3}{2}}$. Although the measurements are not all compatible within the quoted errors, our set is in general in rather good agreement with the previous determinations.

In conclusion, we have developed a method to measure the diffusion coefficient of mercury in a generic gas at room temperature and low pressure, which led to a consistent set of measurements for nine gases, including helium-3 and oxygen, which were not measured before.

ACKNOWLEDGMENTS

APPENDIX: COMPUTATION OF THE LONGITUDINAL RELAXATION RATE FOR A CYLINDRICAL CELL IN UNIFORM MAGNETIC GRADIENTS

In the motional narrowing regime of spin relaxation, the effect of a random perturbation can be evaluated with the help of second-order perturbation theory [28]. The longitudinal depolarization rate Γ_1 can be written as

$$\Gamma_1 = \gamma^2 \int_0^\infty \text{Re}[\langle b^*(0)b(t)\rangle e^{i\omega t}]dt, \tag{A1}$$

where ω is the Larmor angular precession frequency and b is a complex noise representing the transverse components of the magnetic field $\vec{B}$. If the main magnetic field is taken to be along x, then $b = B_y + iB_z$.

Now, we have to compute the correlation function of b. Following the work of McGregor [15], we write

$$\langle b^*(0)b(t)\rangle = \int_V \frac{1}{V} d\overrightarrow{r_0} \int_V d\vec{r}\, b^*(\overrightarrow{r_0})b(\vec{r})\pi(\vec{r}, t \mid \overrightarrow{r_0}), \tag{A2}$$

where V is the volume of the cell and $\pi(\vec{r}, t \mid \vec{r}_0)$ is the conditional probability (or propagator) for an atom to be at $\vec{r}$ at the time t given that it started at the position $\vec{r}_0$ at $t = 0$.

In the case of the diffusive regime, it is possible to obtain an analytical expression for the propagator. Indeed, the propagator follows the diffusion equation

$$D\Delta\pi(\vec{r}, t \mid \overrightarrow{r_0}) = \frac{\partial}{\partial t}\pi(\vec{r}, t \mid \overrightarrow{r_0}), \tag{A3}$$

where D is the diffusion coefficient. Then, $\pi(\vec{r}, t \mid \vec{r}_0)$ must satisfy the initial condition

$$\pi(\vec{r}, t = 0 \mid \overrightarrow{r_0}) = \delta(\vec{r} - \overrightarrow{r_0}), \tag{A4}$$

and the boundary condition on the cell walls

$$\vec{\nabla}\pi(\vec{r}, t \mid \overrightarrow{r_0}) \cdot \vec{n} = 0, \tag{A5}$$

where $\vec{n}$ is the vector normal to the surface.

Let us consider the diffusion within a cylindrical cell of length L and radius R where its axis is aligned with the x axis. A convenient coordinate system is the cylindrical one (ρ, θ, x): let us use the method of separation of variables and search for solutions in the form of

$$f(\rho, \theta, x, t) = \mathcal{R}(\rho)\mathcal{A}(\theta)\mathcal{X}(x)\mathcal{T}(t).$$

When injecting this equation into the diffusion equation, we obtain

$$\mathcal{R}(\rho) = \mathcal{R}_0 J_n(k\rho), \quad \mathcal{A}(\theta) = \mathcal{A}_0 e^{im\theta},$$
$$\mathcal{X}(x) = \mathcal{X}_1 \cos(lz) + \mathcal{X}_2 \sin(lz),$$
$$\mathcal{T}(t) = \mathcal{T}_0 \exp[-D(k^2 + l^2)t],$$

where J_n is the cylindrical Bessel function of order n.

The boundary conditions (A5) on the cell imposes that k and n should be integers and

$$\mathcal{R}(\rho) = \mathcal{R}_0 J_n\left(x_{nk}\frac{\rho}{R}\right), \tag{A6}$$

$$\mathcal{X}(x) = \mathcal{X}_1 \cos\left(n\pi\frac{z}{L}\right) + \mathcal{X}_2 \sin\left(n\pi\frac{z}{L}\right), \tag{A7}$$

where x_{nk} is the kth zero of the J_n derivative.

The general solution of the diffusion equation in the cylindrical cell is then the linear combination of all the solutions found above, whose coefficients can be computed using the initial condition (A4). In the end we obtain the conditional probability $\pi(\vec{r}, t \mid \overrightarrow{r_0})$:

$$\pi(\vec{r}, t \mid \overrightarrow{r_0}) = \pi_\perp(\rho, \theta, t \mid \rho_0, \theta_0)\pi_\parallel(x, t \mid x_0), \tag{A8}$$

with

$$\pi_\perp(\rho, \theta, t \mid \rho_0, \theta_0) = \frac{1}{2\pi R^2} \sum_{m\in\mathbb{Z}, k\in\mathbb{N}^*} \Lambda_{mk,1}^{-1} J_m\left(x_{mk}\frac{\rho}{R}\right) J_m\left(x_{mk}\frac{\rho_0}{R}\right) e^{im(\theta-\theta_0)} e^{-D\left(\frac{x_{mk}}{R}\right)^2|t|},$$

$$\pi_\parallel(x, t \mid x_0) = \frac{1}{L} + \frac{2}{L}\sum_{n=2,4,\dots} \cos\left(n\pi\frac{x}{L}\right)\cos\left(n\pi\frac{x_0}{L}\right)e^{\left(-D\frac{n\pi}{L}\right)^2|t|} + \frac{2}{L}\sum_{n=1,3,\dots} \sin\left(n\pi\frac{x}{L}\right)\sin\left(n\pi\frac{x_0}{L}\right)e^{\left(-D\frac{n\pi}{L}\right)^2|t|},$$

with $\Lambda_{mk,\alpha} = \frac{1}{R^{\alpha+1}}[\int_0^R J_m(x_{mk}\frac{\rho}{R})\rho^\alpha d\rho]$.

Let us now return to the expression (A2). In the case where b is a linear function of the spatial coordinates, we have

$$b(\vec{r}) = \frac{\partial b}{\partial x}x + \frac{\partial b}{\partial y}y + \frac{\partial b}{\partial z}z. \tag{A9}$$

By injecting Eq. (A9) in Eq. (A2) and using Eq. (A8), we get

$$\langle b^*(0)b(t)\rangle = \left|\frac{\partial b}{\partial x}\right|^2 \langle x(0)x(t)\rangle + \left(\left|\frac{\partial b}{\partial y}\right|^2 + \left|\frac{\partial b}{\partial z}\right|^2\right)\langle z(0)z(t)\rangle, \tag{A10}$$

where

$$\langle x(0)x(t)\rangle = \frac{8L^2}{\pi^4}\sum_{n=1,3,\dots}\frac{1}{n^4}e^{-D\left(\frac{n\pi}{L}\right)^2|t|}, \quad \langle z(0)z(t)\rangle = R^2\sum_{k\in\mathbb{N}^*}\frac{\Lambda_{1k,2}}{\Lambda_{1k,1}}e^{-D\left(\frac{x_{1k}}{R}\right)^2|t|}.$$

Finally, by injecting Eq. (A10) into Eq. (A1), we obtain the general expression for the longitudinal relaxation rate for a cylindrical cell immersed in a uniform gradient:

$$\Gamma_1 = \frac{\gamma^2 D}{\omega^2}\left[\left|\frac{\partial b}{\partial x}\right|^2\sum_{n=1,3,\dots}\frac{\left(\omega\frac{L^2}{D}\right)^2}{\left(\omega\frac{L^2}{D}\right)^2+(n\pi)^4}\frac{8}{(n\pi)^2} + \left(\left|\frac{\partial b}{\partial y}\right|^2 + \left|\frac{\partial b}{\partial z}\right|^2\right)\sum_{k\in\mathbb{N}^*}\frac{\left(\omega\frac{R^2}{D}\right)^2}{\left(\omega\frac{R^2}{D}\right)^2+x_{1k}^4}\frac{2}{x_{1k}^2-1}\right]. \tag{A11}$$

Now, this general expression can be simplified for specific shapes of the magnetic field. In particular, if $\frac{\partial b}{\partial x} = 0$ [valid in the experimental setup used in this study, see Eq. (5)], Eq. (A11) simplifies into Eq. (2) given that

$$G^2 = \langle(\vec{\nabla}B_y)^2 + (\vec{\nabla}B_z)^2\rangle = \left|\frac{\partial b}{\partial x}\right|^2 + \left|\frac{\partial b}{\partial y}\right|^2 + \left|\frac{\partial b}{\partial z}\right|^2. \tag{A12}$$

---

[1] H. Y. Carr and E. M. Purcell, Phys. Rev. **94**, 630 (1954).

[2] R. Barbé, M. Leduc, and F. Laloë, J. Phys. **35**, 699 (1974).

[3] M. Bock, Magn. Reson. Med. **38**, 890 (1997).

[4] M. E. Hayden, G. Archibald, K. M. Gilbert, and C. Lei, J. Magn. Reson. **169**, 313 (2004).

[5] R. H. Acosta, L. Agulles-Pedrós, S. Komin, D. Sebastiani, H. W. Spiess, and P. Blümler, Phys. Chem. Chem. Phys. **8**, 4182 (2006).

[6] K. C. Hasson, G. D. Cates, K. Lerman, P. Bogorad, and W. Happer, Phys. Rev. A **41**, 3672 (1990).

[7] X. Liu, C. Chen, T. Qu, K. Yang, and H. Luo, Sci. Rep. **6**, 24122 (2016).

[8] T. R. Marrero and E. A. Mason, J. Phys. Chem. Ref. Data **1**, 3 (1972).

[9] N. Bloembergen, E. M. Purcell, and R. V. Pound, Phys. Rev. **73**, 679 (1948).

[10] M. Bouchiat, T. Carver, and C. Varnum, Phys. Rev. Lett. **5**, 373 (1960).

[11] R. Gamblin and T. Carver, Phys. Rev. **138**, A946 (1965).

[12] L. D. Schearer and G. K. Walters, Phys. Rev. **139**, A1398 (1965).

[13] A. Redfield, Adv. Magn. Reson. **1**, 1 (1965).

[14] G. D. Cates, S. R. Schaefer, and W. Happer, Phys. Rev. A **37**, 2877 (1988).

[15] D. D. McGregor, Phys. Rev. A **41**, 2631 (1990).

[16] R. Golub, R. M. Rohm, and C. M. Swank, Phys. Rev. A **83**, 023402 (2011).

[17] G. Pignol, M. Guigue, A. Petukhov, and R. Golub, Phys. Rev. A **92**, 053407, (2015).

[18] M. Guigue, G. Pignol, R. Golub, and A. K. Petukhov, Phys. Rev. A **90**, 013407, (2014).

[19] See Supplemental Material at http://link.aps.org/supplemental/10.1103/PhysRevA.106.062815 for files containing the reduced data and the summary plot for each run.

[20] J. O. Hirschfelder, C. F. Curtiss, and R. B. Bird, *Molecular Theory of Gases and Liquids* (Wiley, New York, 1955).

[21] W. J. Massman, Atmos. Environ. **33**, 453 (1999).

[22] P. J. Gardner, P. Pang, and S. R. Preston, J. Chem. Eng. Data **36**, 265 (1991).

[23] H. B. Spencer, J. M. Toguri, and J. A. Kurtis, Can. J. Chem. **47**, 2197 (1969).

[24] K. Nakayama, Jpn. J. Appl. Phys. **7**, 1114 (1968).

[25] B. E. Poling, J. M. Prausnitz, and J. P. O'Connell, *The Properties of Gases and Liquids,* 5th Ed. (McGraw-Hill, New York, 2001).

[26] S. Chapman and T. G. Cowling, *The Mathematical Theory of Non-Uniform Gases* (Cambridge University Press, London, 1939).

[27] C. R. Mueller and R. P. Marchi, J. Chem. Phys. **38**, 745 (1963).

[28] A. Abragam, *The Principles of Nuclear Magnetism* (Clarendon Press, Oxford, 1961).